Shock-Fitting Bicharacteristic Algorithm for Three-Dimensional Scarfed Nozzle Flowfields

Joseph Vadyak* and Joe D. Hoffman†
Purdue University, West Lafayette, Indiana

The flowfield in an axisymmetric scarfed propulsive nozzle is computed using a pentahedral bicharacteristic method devised for steady three-dimensional flows. For cases in which the nozzle contour has a slope discontinuity that causes a flow compression, then the resulting shock wave system is computed using a three-dimensional discrete shock wave fitting procedure. The shock wave system is included in the computation until shock waves emanating from opposite sides of the nozzle approximately intersect. The culmination of the present research endeavor is the development of a production-type computer program capable of predicting the flowfield and resultant forces and moments for a variety of axisymmetric scarfed nozzle configurations. Computed solutions are presented to illustrate application of the analysis.

Nomenclature

a	= sonic speed
c	= velocity of divergence of Mach conoid
l	= unit vector along a space curve
M	= Mach number
n	= unit vector normal to a characteristic surface
n_b	= unit vector normal to a solid boundary
n_s	= unit vector normal to a shock surface
P	= pressure
q	= velocity magnitude
r	= radial position
t	= time or time-like parameter
t	= unit vector along a space curve
T	= temperature
u,v,w	= x,y,z velocity components, respectively
V	= velocity vector
x,y,z	= Cartesian coordinates
α_i,β_i	= parametric unit vectors
γ	= specific heat ratio
δ	= deflection angle
θ	= parametric angle, or polar angle
ρ	= density
σ	= unit vector in a plane normal to the nozzle exit lip

Subscripts

d	= downstream conditions
i,j,k	= Cartesian indices (1-3)
u	= upstream conditions
x,y,z	= partial differential with respect to x,y,z

Introduction

THE purpose of this investigation[1] was to develop a method for calculating the three-dimensional supersonic flowfield in scarfed propulsive nozzles. The two classes of scarfed nozzle configurations considered in the present study are illustrated in Fig. 1. Figure 1a depicts the case in which the nozzle contour has continuous slope. The nozzle geometry is assumed to be axisymmetric. The internal flowfield will be axisymmetric if Mach waves emanating from point A on the exit lip do not intersect the opposite side of the nozzle. If the Mach waves do intersect the opposite side of the nozzle, as illustrated, then cross flow develops and the latter portion of the internal flowfield will become three dimensional. Figure 1b depicts the case in which the nozzle contour has a slope discontinuity contained in the axial station at which scarfing initiates. In this case, a shock wave system is generated as shown. The shocks emanating from opposite sides of the nozzle eventually intersect and form a normal shock in the core of the flowfield. The flow will transition from supersonic to subsonic as it passes through the normal shock wave.

The equations of motion for steady three-dimensional supersonic flow may be classified as a system of hyperbolic quasilinear partial differential equations of first order. In the present investigation, those equations are solved using a pentahedral bicharacteristic algorithm devised for steady three-dimensional flows. For cases in which the nozzle

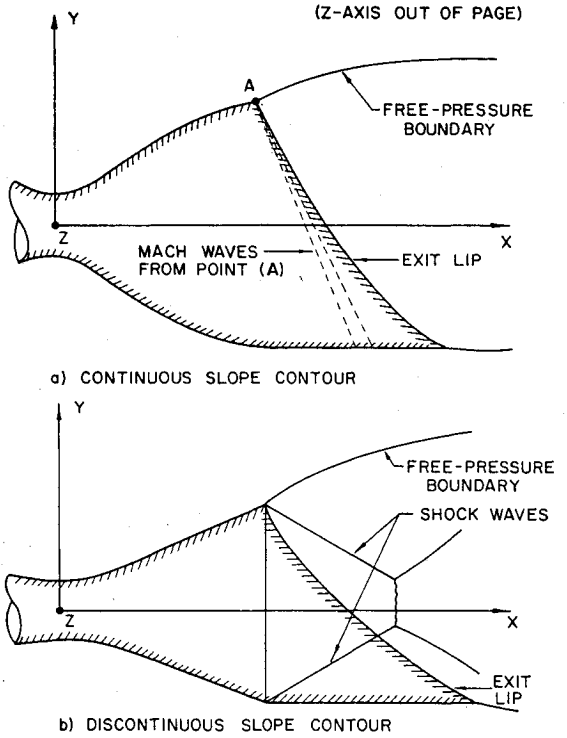

Fig. 1 Scarfed nozzle configurations.

Presented as Paper 81-0258 at the AIAA 19th Aerospace Sciences Meeting, St. Louis, Mo., Jan. 12-15, 1981; submitted March 4, 1981; revision received April 28, 1982.

*Visiting Assistant Professor of Mechanical Engineering; presently, Scientist, Advanced Flight Sciences Department, Lockheed-Georgia Co., Marietta, Ga. Member AIAA.

†Professor of Mechanical Engineering. Member AIAA.

contour has a slope discontinuity contained in the axial station where scarfing initiates, the resulting shock wave system is computed using a three-dimensional discrete shock-fitting procedure. The shock wave is assumed to be attached to the nozzle wall. The shock system is included in the computation until shocks emanating from opposite sides of the nozzle approximately intersect. At this stage, the annular flow region downstream of the shock wave at this station is used as initial data for the remainder of the computation, and the solution is continued as far as this initial data allows. The subsonic core flow downstream of the normal shock wave is not computed. It is assumed in the present analysis that the jet expands into a quiescent medium with no mixing.

A prior effort at computing scarfed nozzle internal flows was made by Buchman and Sternfeld[2] who employed a two-dimensional characteristic procedure. This analysis is, of course, applicable only to nozzle configurations in which the internal flow remains axisymmetric. Three-dimensional supersonic nozzle flow algorithms have been developed by Ransom et al.,[3] Cline and Hoffman,[4] and Dash and DelGuidice.[5] Ransom et al. developed a second-order bicharacteristic algorithm for computing isentropic three-dimensional nozzle flows assuming the exclusion of strong shocks. Cline and Hoffman extended the analysis of Ref. 3 to include the effects of finite-rate thermochemical reactions. In both of these analyses, the nozzle exit plane was assumed to be orthogonal to the nozzle axis. Consequently, they are not applicable to scarfed nozzle computations. Dash and DelGuidice developed a three-dimensional nozzle flow analysis based on a reference plane quasicharacteristic method. This analysis was not, however, directed at scarfed nozzle flowfield predictions.

Gas Dynamic Model

The gas dynamic model is based on the following assumptions: 1) steady flow, 2) a simple system in thermodynamic equilibrium, and 3) inviscid flow with negligible thermal conduction. The governing equations consist of the continuity equation, the component momentum equations, the energy equation, and the thermal and caloric equations of state.

For steady three-dimensional flow, the equations of motion are given by

$$\rho u_x + \rho v_y + \rho w_z + u\rho_x + v\rho_y + w\rho_z = 0 \tag{1}$$

$$\rho u u_x + \rho v u_y + \rho w u_z + P_x = 0 \tag{2}$$

$$\rho u v_x + \rho v v_y + \rho w v_z + P_y = 0 \tag{3}$$

$$\rho u w_x + \rho v w_y + \rho w w_z + P_z = 0 \tag{4}$$

$$uP_x + vP_y + wP_z - a^2(u\rho_x + v\rho_y + w\rho_z) = 0 \tag{5}$$

Representations for the thermal equation of state and sonic speed are given by

$$T = T(P,\rho) \tag{6}$$

$$a = a(P,\rho) \tag{7}$$

Characteristic Equations

Systems of hyperbolic partial-differential equations in three independent variables have the property that there exist surfaces in three-dimensional space on which linear combinations of the original differential equations can be formed that contain derivatives only in the surfaces themselves. These special surfaces are called characteristic surfaces, and the linear combinations of the original differential equations are interior differential operators known as compatibility relations.

For steady three-dimensional supersonic flow, two families of characteristic surfaces exist. One family of characteristic surfaces consists of the stream surfaces which are surfaces composed of streamlines. A streamline may be represented by

$$\frac{dx}{dt} = u \qquad \frac{dy}{dt} = v \qquad \frac{dz}{dt} = w \tag{8}$$

where t is the time of travel of a fluid particle along the streamline. The compatibility relations that are applicable on the stream surfaces are given by

$$\frac{dP}{dt} - a^2 \frac{d\rho}{dt} = 0 \tag{9}$$

$$\rho u \frac{du}{dt} + \rho v \frac{dv}{dt} + \rho w \frac{dw}{dt} + \frac{dP}{dt} = 0 \tag{10}$$

In Eqs. (9) and (10), the operator $d(\ )/dt$ represents the directional derivative along a streamline.

The second family of characteristic surfaces consists of the wave surfaces. The envelope of all wave surfaces at a point forms a conoid known as the Mach conoid. The Mach conoid may be represented locally by a right-circular cone known as the Mach cone. The line of contact between a particular wave surface and the Mach conoid is known as a bicharacteristic.

Butler[6] developed a parametric form of representing a bicharacteristic and the wave surface compatibility relation applicable along it. Butler's bicharacteristic parameterization is given by

$$dx_i = (u_i + c\alpha_i \cos\theta + c\beta_i \sin\theta)\,dt \quad (i = 1,2,3) \tag{11}$$

where t is the time of travel of a fluid particle along the streamline that is the axis of the Mach cone, θ is a parametric angle denoting a particular element of the Mach cone and has the range $0 \le \theta \le 2\pi$, and c is given by

$$c^2 = q^2 a^2 / (q^2 - a^2) \tag{12}$$

The vectors α_i and β_i in Eq. (11) are parametric unit vectors with α_i, β_i, and u_i/q $(i = 1,2,3)$ forming an orthonormal set (see Fig. 2). The corresponding parametric form of the wave surface compatibility relation is given by

$$\frac{dP}{dt} + \rho c(\alpha_i \cos\theta + \beta_i \sin\theta)\frac{du_i}{dt} = -\rho c^2(\alpha_i \sin\theta - \beta_i \cos\theta) \times (\alpha_j \sin\theta - \beta_j \cos\theta)\frac{\partial u_i}{\partial x_j} \tag{13}$$

In Eq. (13), the operator $d(\ )/dt$ represents differentiation in the bicharacteristic direction, and the terms $\partial u_i/\partial x_j$, which are called cross derivatives, represent differentiation in the wave surface normal to the bicharacteristic direction.

In addition to the preceding relations, Butler also developed another relation that is applicable along a streamline. This relation, which is an independent linear combination of the system of differential equations, is given by

$$\frac{dP}{dt} = -\rho c^2(\alpha_i \alpha_j + \beta_i \beta_j)\frac{\partial u_i}{\partial x_j} \tag{14}$$

where the operator $d(\ )/dt$ denotes differentiation along a streamline.

An any point in the flowfield, there exists an infinite number of stream surfaces and wave surfaces. The number of independent compatibility relations cannot exceed the number of independent equations of motion. Consequently, it is necessary to determine which of the possible combinations of the compatibility relations form an independent set. Rusanov[7] has shown for steady three-dimensional isentropic flow that two of the stream surface compatibility relations applied along a stream surface and the single wave surface compatibility relation applied along three different wave

surfaces form an independent set of five characteristic relations.

Unit Processes

General Considerations

A variety of unit processes are employed in the computation of the flowfield. The unit processes may be classified into six major types: interior point, solid boundary point, field-shock wave point, solid body-shock wave point, exit lip point, and free-pressure boundary point. The basic interior and solid boundary point unit processes applied to planar initial-value surfaces have been employed in a previous investigation by Ransom et al.[3] The shock point unit processes have been applied in aircraft inlet calculations by Vadyak and Hoffman.[8] The exit lip point and free-pressure boundary point unit processes were devised specifically for this investigation.

In the overall algorithm, an inverse marching scheme is employed. The solution is obtained on a series of space-like surfaces, each being approximately centered about the x axis which is the longitudinal axis of the nozzle. The distance between successive solution surfaces is determined by the Courant-Friedrichs-Lewy (CFL) stability criterion. Marching is performed in the local time-like direction at each solution point. Consequently, a given solution surface has some degree of curvature, and is approximately orthogonal to the streamlines passing through it.

Interior and Solid Boundary Point Unit Processes

The flow computations for the interior point unit process are performed in a local coordinate system which is oriented such that its x axis is aligned with the local time-like direction; that is, it coincides with the streamline passing through the point under consideration. The local x axis is the direction along which marching is performed. Before the interior point unit process is initiated, all position and velocity vectors are transformed from the base coordinate system (see Fig. 1) to the local coordinate system using a coordinate rotation. In the following discussion of the interior point unit process, the coordinate system referred to is the local coordinate system.

The computational network used in determining an interior point is illustrated in Fig. 2. Points (1)-(4) represent the intersection points of four rearward-running bicharacteristics with the initial-value surface, point (5) is the streamline intersection point with the initial-value surface, and point (6) is the solution point. The distance between the initial-value and solution surfaces is determined by the CFL criterion. The interior point unit process is an explicit predictor-corrector algorithm. The corrector is iterated to convergence.

The interior point unit process is initiated by determining the location of the solution point. The coordinates of point (6) are determined by extending the streamline from point (5) to the solution surface using the following finite-difference form of Eq. (8).

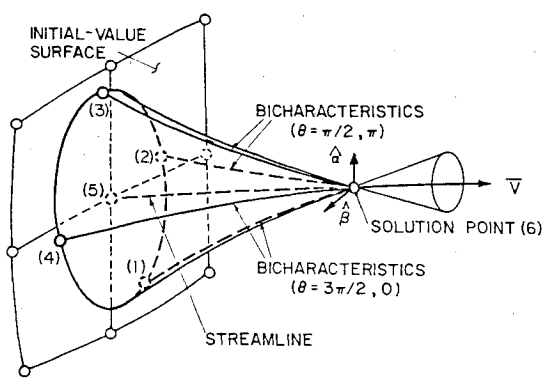

Fig. 2 Interior point computational network.

$$x_i(6)-x_i(5)=\tfrac{1}{2}[u_i(5)+u_i(6)][t(6)-t(5)] \quad (i=1,2,3) \quad (15)$$

Interpolated flow property values at point (5) are used in the integration, even though point (5) is a known field point. As shown by Ransom et al.,[3] this interpolation is required to produce a stable numerical scheme. The interpolated flow property values are obtained from the following quadratic trivariate interpolation polynomial

$$f(x,y,z)=a_1+a_2y+a_3z+a_4yz+a_5y^2+a_6z^2+a_7xy+a_8xz \quad (16)$$

where $f(x,y,z)$ denotes a general function of the coordinates x, y, and z, and the coefficients a_i (i=1-8) are obtained from a least squares fit of points in the region of point (5).

With the location of the solution point determined, four bicharacteristics are extended from the solution point back to the initial-value surface, intersecting this surface at points (1)-(4). The initial-value surface is represented by the quadric surface formulation

$$x^2=b_1+b_2y+b_3z+b_4yz+b_5y^2+b_6z^2 \quad (17)$$

where x, y, and z are coordinates of a point on the initial-value surface, and the coefficients b_i (i=1-6) are determined from a least squares fit of points on the initial-value surface. To determine the bicharacteristic initial-value surface intersection points, an iterative procedure is employed. The procedure, described in detail in Ref. 1, requires using the following finite-difference form of Eq. (11).

$$dx_i(k)=\tfrac{1}{2}\{u_i(k)+u_i(6)+[c(k)+c(6)][\alpha_i\cos\theta(k)+\beta_i\sin\theta(k)]\}dt(k) \quad (i=1,2,3) \quad (18)$$

The index k in Eq. (18) denotes the bicharacteristic initial-value surface intersection points illustrated in Fig. 2, and has a range of 1-4, corresponding to the $\theta(k)$ values of 0, $\pi/2$, π, and $3\pi/2$, respectively. The flow properties at points (1)-(4) are determined by interpolation using Eq. (16).

Once the positions of and the flow properties at points (1)-(5) have been determined, the system of nonlinear compatibility equations is solved to obtain the five flow properties $u(6)$, $v(6)$, $w(6)$, $P(6)$, and $\rho(6)$. Two of the five required compatibility equations are given by Eqs. (9) and (10). These equations are written in finite-difference form by replacing the derivatives with simple differences, and by replacing the coefficients of the derivatives with the arithmetic average of the coefficients at the solution point and at the appropriate point in the initial-value surface. To obtain the remaining three required compatibility equations, appropriate linear combinations of the wave surface compatibility relation, Eq. (13), applied along each of the four bicharacteristics, and Eq. (14), applied along the streamline, are formed. One independent linear combination of the compatibility equations is obtained by subtracting the finite-difference form of Eq. (13) evaluated for $\theta=\pi$ from the finite-difference form of Eq. (13) evaluated for $\theta=0$. Another independent linear combination is obtained by subtracting the finite-difference form of Eq. (13) evaluated for $\theta=3\pi/2$ from the finite-difference form of Eq. (13) evaluated for $\theta=\pi/2$. The final independent linear combination is obtained by subtracting the finite-difference form of Eq. (14) from the sum of the finite-difference forms of Eq. (13) evaluated for $\theta=0$ and $\theta=\pi/2$. The resulting compatibility equations do not contain cross derivatives at the solution point [i.e., all terms containing $\partial u_i/\partial x_j(6)$ are eliminated]. These five equations are solved using Gauss elimination to obtain the five dependent flow properties at the solution point. For the predictor, the flow property values at the solution point appearing in the coefficients of the difference equations are equated to those at point (5). For the corrector, the flow property values at point

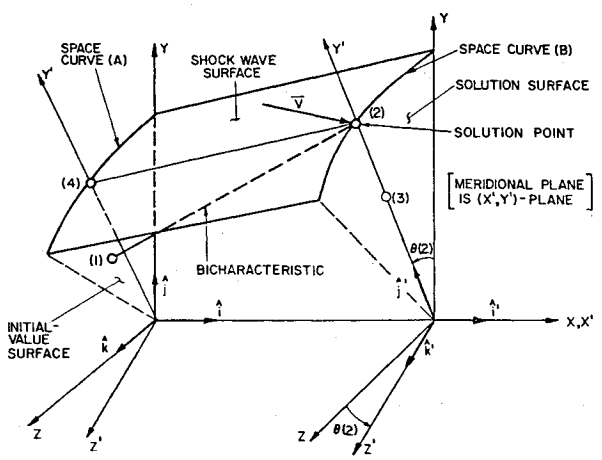

Fig. 3 Field-shock point computational network.

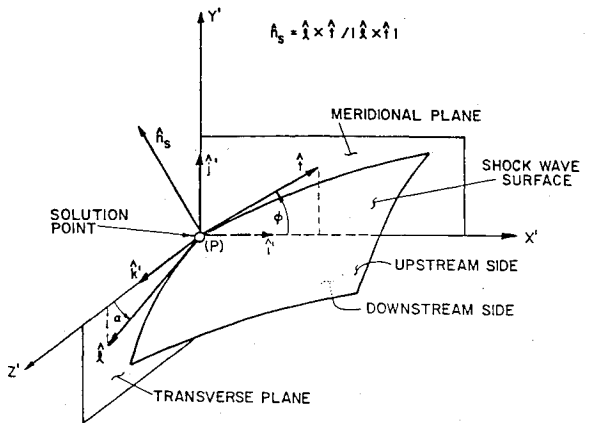

Fig. 4 Unit vectors for shock surface specification.

(6) obtained on the previous iteration are used. The resulting scheme has second-order accuracy,[3] and does not violate the domain of dependence at the solution point.

The unit process to obtain the solution at a solid boundary point is almost identical to the interior point unit process. Here, however, both points (5) and (6) are constrained to lie on the solid boundary. Moreover, point (4) corresponding to the bicharacteristic with $\theta = 3\pi/2$ is not inside the flowfield, so the corresponding compatibility relation is not employed. That equation is replaced by the flow tangency condition

$$u_i(6)n_{bi}(6) = 0 \tag{19}$$

where $n_{bi}(6)$ $(i = 1,2,3)$ is the unit normal to the solid boundary at point (6).

Once convergence has been attained, the position vector of and the velocity vector at the solution point are transformed from the local coordinate system to the base coordinate system.

Field-Shock Wave Point Unit Process

The field-shock wave point scheme is a predictor-corrector algorithm with the corrector being iterated to convergence. Figure 3 depicts the field-shock wave point computational network. The intersection of the shock wave with the initial-value surface and the solution surface defines curves A and B, respectively. The solution point, at which the upstream properties are known, is denoted by point (2). A rearward-running bicharacteristic is extended from point (2) to the initial-value surface, intersecting this surface at point (1). Point (3) is an adjacent interior point used to define the meridional plane of point (2). Point (4) is the intersection of curve A with the meridional plane of point (2).

A local Cartesian coordinate system (x',y',z') is used to describe the orientation of the shock surface. The coordinate x' is coincident with the x axis, y' is the radial direction through point (2), and z' is normal to the (x',y') plane. As shown in Fig. 4, the shock surface orientation at a point (P) is described by the set of three unit vectors: n_s, l, and t. The vector n_s is normal to the shock surface at point (P). The vector t is tangent to the shock at point (P), lies in the meridional plane of that point, and subtends an angle ϕ with the x' axis. The vector l is tangent to the shock at point (P), lies in the transverse plane, and subtends an angle α with the z' axis. Expressions for the three unit vectors are given by

$$t = \cos\phi i' + \sin\phi j' \tag{20}$$

$$l = \sin\alpha j' + \cos\alpha k' \tag{21}$$

$$n_s = l \times t / |l \times t| \tag{22}$$

The shock point unit process is initiated by locating the solution point. The solution point is selected arbitrarily to lie in the meridional plane of point (3). The radial position of the solution point is obtained from

$$r(2) = r(4) + [x(2) - x(4)]\tan\{\tfrac{1}{2}[\phi(2) + \phi(4)]\} \tag{23}$$

where on the initial application of this equation, $\phi(2)$ is equated to $\phi(4)$. At point (4), $r(4)$, and $\phi(4)$ are determined by interpolation using quadratic polynomials written in terms of the polar angle $\theta = \tan^{-1}(z/y)$.

At this stage, the shock normal unit vector n_s at the solution point is found by using Eq. (22). The tangential vectors t and l are obtained by use of the current values of $\phi(2)$ and $\alpha(2)$ in Eqs. (20) and (21), respectively. The value of $\alpha(2)$ is approximated by equating it to $\alpha(4)$ and, thereby, is lagged by one marching step in the computation. The angle $\alpha(2)$ is determined from

$$\alpha(2) = \tan^{-1}\left(\frac{l}{r}\frac{\mathrm{d}r}{\mathrm{d}\theta}\right)\Big|_{\theta(2)} \tag{24}$$

where the analytical form of $r(\theta)$ used in this equation is obtained by curve fitting points along curve A.

The local Hugoniot relations are then applied at point (2) to obtain the downstream flow properties $u(2)$, $v(2)$, $w(2)$, $P(2)$, and $\rho(2)$. Next, a rearward-running bicharacteristic is extended from the solution point back to the initial-value surface, intersecting this surface at point (1). The coordinates of point (1) are obtained by an iterative procedure which requires using a finite-difference form of Eq. (11) evaluated for the parametric angle $\theta = \pi/2$. The flow properties at point (1) are obtained by interpolation using Eq. (16).

At this stage, the wave surface compatibility equation corresponding to the parametric angle $\theta = \pi/2$ is applied between points (1) and (2). The appropriate equation is obtained by writing Eq. (13) evaluated for $\theta = \pi/2$ in finite-difference form and solving for the pressure at point (2). Denote this pressure as $P^*(2)$. The resulting equation contains cross derivatives at both points (1) and (2). The cross derivatives at point (2) are approximated by equating them to those at point (1).

The pressure $P(2)$ is calculated from the local Hugoniot equations, whereas, the pressure $P^*(2)$ is calculated from the wave surface compatibility relation. The difference between $P(2)$ and $P^*(2)$ is driven to within a specified tolerance of zero using the secant method with iteration being performed on the shock wave angle $\phi(2)$.

Solid Body-Shock Wave Point Unit Process

This unit process is used to obtain the flow properties downstream of the shock wave at a point where the shock intersects a solid boundary. This unit process is used to determine the solution at the points on the solid boundary on

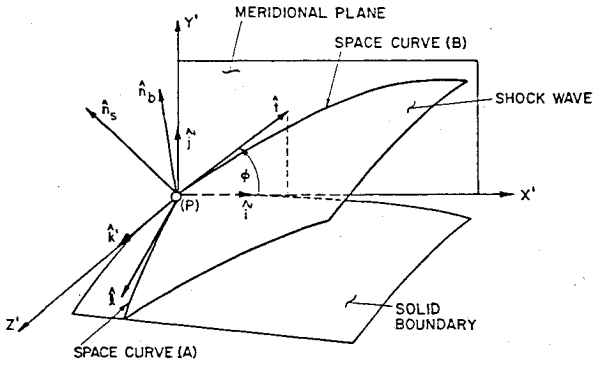

Fig. 5 Solid body-shock point computational network.

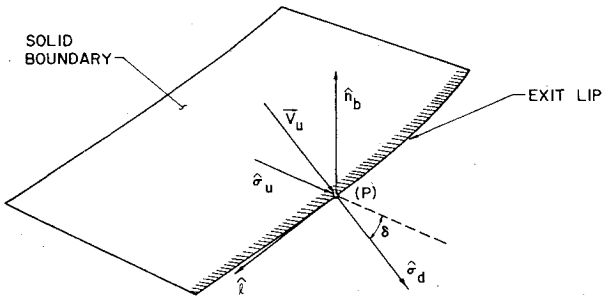

Fig. 6 Exit lip point computational network.

the downstream side of the body generated shock wave when the nozzle contour has a slope discontinuity. Consequently, the solution points lie on the ring defined by the intersection of the upstream and downstream nozzle sections.

The computational network used in this scheme is depicted in Fig. 5 where a typical solution point is denoted by point (P). The intersections of the shock wave with the solid boundary and the meridional plane passing through point (P) define curves A and B, respectively. The unit vectors tangent to curves A and B at point (P) are denoted by l and t, respectively. The unit vectors normal to the shock wave and the solid boundary at point (P) are denoted by n_s and n_b, respectively.

As for the field-shock wave point unit process, the vectors l, t, and n_s are referenced to the local coordinate system (x',y',z'), where x', y', and z' have the same definitions as noted before. The tangential unit vector t again lies in the meridional plane and is defined by Eq. (20). The tangential unit vector l along curve A is defined by

$$l=\frac{dx'}{ds}i'+\frac{dy'}{ds}j'+\frac{dz'}{ds}k' \tag{25}$$

where ds denotes the differential arc length along curve A.

The solid body-shock wave point unit process is initiated by determining the unit vectors n_b and l. An assumption is then made for the angle ϕ in Eq. (20), and the unit vector n_s is computed using Eq. (22). The local Hugoniot relations are applied to obtain the downstream flow properties at point (P). The velocity normal to the wall and downstream of the shock wave is then computed and relaxed to within a specified tolerance of zero by varying the shock wave angle ϕ using the secant iteration method.

Exit Lip Point Unit Process

The exit lip point unit process is used to obtain the flow properties downstream of the expansion fan centered at the exit lip at a point on the exit lip. The computational network used in this unit process is presented in Fig. 6, where a typical solution point is denoted by point (P). The outward unit normal vector to the solid boundary at point (P) is denoted by n_b. The unit vector tangent to the exit lip at point (P) is denoted by l. The upstream velocity vector at point (P), which is tangent to the solid boundary, is denoted by V_u. The unit vectors σ_u and σ_d are in a plane which is normal to the tangential vector l at point (P). The angle between σ_u and σ_d is denoted by δ.

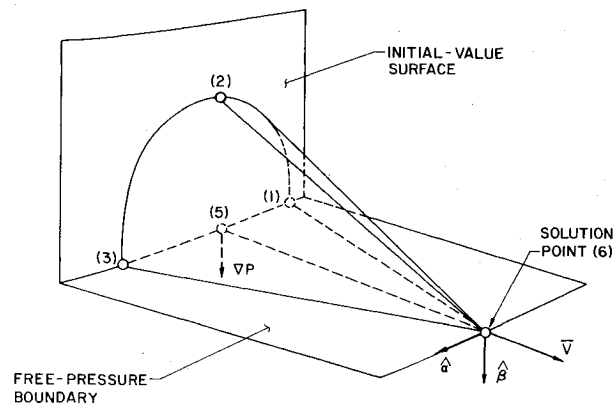

Fig. 7 Free-pressure boundary point computational network.

Before the exit lip point unit process is applied, the position of the exit lip point and the upstream flow properties at that point are determined by the application of a modified solid boundary point unit process. The exit lip point unit process is then applied to obtain the downstream properties after the flow expansion (or compression) has occurred. The downstream flow properties are obtained by performing a two-dimensional Prandtl-Meyer flow analysis in the plane normal to the exit lip at the solution point (i.e., in a plane containing the unit vectors σ_u and σ_d).

The exit lip point unit process is initiated by determining the unit vectors n_b and l. The vector l is found from

$$l=\frac{dx}{ds}i+\frac{dy}{ds}j+\frac{dz}{ds}k \tag{26}$$

where ds is the differential arc length along the exit lip curve. The unit vector σ_u, which is tangent to the solid boundary and normal to the exit lip, is computed using

$$\sigma_u=n_b\times l/|n_b\times l| \tag{27}$$

The upstream velocity components along the σ_u and l directions are then determined.

At this stage, the unit vector σ_d is computed. The unit vector σ_d is contained in the plane normal to the exit lip, and subtends the angle δ with the vector σ_u. The deflection angle δ is determined by the use of a Prandtl-Meyer analysis that is applied in the plane normal to the exit lip. It is assumed that the total enthalpy and the velocity component tangent to the edge are conserved in the expansion process, and that the flow is locally isentropic at the exit lip solution point. The pressure downstream of the expansion fan is assumed to equal the ambient pressure.

Once the deflection angle δ has been computed, the unit vector σ_d may be determined. Then, using the ambient pressure in conjunction with the deflection angle gives the downstream density, enthalpy, and velocity components in the σ_d direction. The velocity components in the σ_d direction may then be added to the velocity components in the l direction to obtain the downstream velocity vector.

The case in which the ambient pressure is somewhat greater than the upstream pressure at the exit lip point may also be computed by this method, however, special constraints are imposed on the deflection angle in this case.

Free-Pressure Boundary Point Unit Process

The free-pressure boundary point unit process is used to obtain the solution at points on the stream surface formed by the jet boundary. It is assumed that the jet expands into a quiescent medium without mixing. The boundary condition used in this unit process is simply that the static pressure on the free-pressure surface be equal to the ambient pressure (i.e., mechanical equilibrium is satisfied). Since the ambient pressure is specified, only four dependent variables have to be obtained by the characteristic analysis: the three velocity components and the density. The flow computations in the free-pressure boundary point scheme are performed in a local coordinate system whose x axis is aligned with the local time-like direction, similar to the interior and solid boundary point algorithms. The computational point network used in the free-pressure boundary point unit process is presented in Fig. 7. The point nomenclature in Fig. 7 is the same as that of Fig. 2.

The free-pressure boundary point unit process is initiated by determining the location of the solution point. This is accomplished using Eq. (15), as was done for the interior and solid boundary point algorithms. With the solution point location obtained, three bicharacteristics are extended from the solution point back to the initial-value surface, intersecting this surface at points (1)-(3). The intersection points are determined using an iterative procedure. This again involves using Eq. (18) applied for θ values of 0, $\pi/2$, and π. The parametric unit vector β_i in Eq. (18) is aligned with the pressure gradient in the initial-value surface since the pressure gradient is normal to the plume surface (a surface of constant pressure). The unit vector α_i is found from the orthonormal relationship between α_i, β_i, and u_i/q $(i=1,2,3)$. The flow properties at points (1)-(3) and point (5) on the quadric initial-value surface are obtained by interpolation using Eq. (16).

At this stage, the system of compatibility relations is solved to obtain the four dependent flow properties $u(6)$, $v(6)$, $w(6)$, and $\rho(6)$. Two of the four required compatibility relations are given by Eqs. (9) and (10). These equations are again written in finite-difference form, however, in this algorithm the pressure derivative along a streamline is identically zero. The two remaining compatibility relations are obtained by forming linear combinations of the wave surface compatibility relation, given by Eq. (13), and Eq. (14). The pressure derivative in Eq. (14) is identically zero in this scheme. These four difference relations are solved by Gauss elimination. A predictor-corrector type algorithm is used, similar to the interior and solid boundary point unit processes. Once convergence has been attained, all vector quantities are transformed from the local to the base coordinate system.

Shock Modified Unit Processes

In some situations during the computation, the interior and solid boundary point unit processes must be applied in a modified form. One such situation is when the Mach cone, with apex at the interior solution point, intersects not only the initial-value surface but also the internal shock and/or a solid boundary. The unit process in this case requires determining the bicharacteristic intersection points with the shock and/or the solid boundary in addition to the intersection points with the initial-value surface. Moreover, flow property values must be determined at all of these points. The procedures used to obtain a solution in cases like this are presented in Ref. 1.

Overall Numerical Algorithm

An inverse marching scheme is employed with the solution being obtained on a series of space-like surfaces. The points on each solution surface represent the intersection points of streamlines which are propagated from the data points specified on the initial-value surface. In addition to the streamline solution points, auxiliary solution points are also obtained at the intersections of a given solution surface with the exit lip. The streamline flow properties upstream and downstream of the exit lip expansion fan are computed. For the case in which the nozzle has a slope discontinuity, solution points are also obtained at the intersection of the shock wave with a solution surface.

Initial Data and Boundary Conditions

The initial data are specified at the axial station where scarfing initiates. The bicharacteristic analysis is then used to determine the flow downstream of that location. The axisymmetric initial data may be specified directly in the computer program by tabular input. Alternatively, the initial data may be generated internally in the computer program using the two-dimensional characteristic analysis documented in Zucrow and Hoffman.[9] That algorithm uses the Sauer transonic flow analysis to generate the sonic initial-value line in the nozzle throat region.

The computer program assumes that the nozzle contour is axisymmetric. The contour radius and corresponding axial position may be entered in tabular form. Alternatively, the contour radius may be represented as a quadratic function of axial position.

The exit lip curve generated by the nozzle scarfing may be specified by one of two methods. If the exit lip is generated by a plane cutting the nozzle, then specifying the axial stations where scarfing initiates and ends is sufficient to define the exit lip. Alternatively, an arbitrary exit lip may be specified by entering the coordinates of points along the exit lip in tabular form.

Integration Step-Size Regulation

The marching step between solution surfaces is determined by the Courant-Friedrichs-Lewy criterion. The CFL criterion mandates that the domain of dependence of the differential equations be contained within the convex hull of the finite-difference network. That is, the Mach cone must be inside the outer periphery of the initial-value surface field points used in formulating the trivariate interpolation polynomial, Eq. (16). The CFL criterion is applied at every streamline point on the initial-value surface, with the actual integration step being chosen as the marching step at the most restrictive point. The use of the same marching step at each point produces a smooth solution surface. The CFL criterion is applied only to streamline points, the shock points being excluded. Moreover, the shock points are ignored in defining the convex hull of the difference network when applying the stability criterion to a streamline point.

Numerical Stability

A stability analysis of the overall nonlinear finite-difference algorithm including the discrete shock-fitting procedure and exit lip expansion procedure was not attempted. Instead, a stability analysis for steady three-dimensional isentropic flow was conducted. Stability of the generalized analysis was verified by actual numerical calculations.

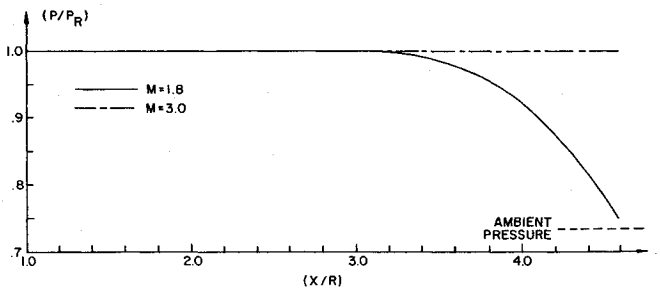

Fig. 8 Wall axial pressure distribution for parallel wall nozzle.

Numerical Results

Selected numerical results are now presented to illustrate the application of the analysis. Nozzle contours with continuous slope and slope discontinuities are considered.

To gain an estimate of the influence of three-dimensional flow effects in the internal flowfield of a scarfed nozzle, computations were performed for a parallel wall nozzle with uniform flow initial data for two entrance Mach numbers. The nozzle has a constant radius which is denoted by R. The exit lip curve is generated by a plane cutting the nozzle. Scarfing initiates at $x=R$ and terminates at $x=4.583R$. For both entrance Mach number cases, the initial-data pressure field is constant at the value P_R. Two different axial flow velocities were used in the computations, giving entrance Mach numbers of 1.8 and 3.0, respectively. The assumed thermodynamic model was that of a thermally and calorically perfect gas.

Wall axial pressure distributions for both entrance Mach number (M) cases are presented in Fig. 8. The illustrated pressure profiles are for the meridian that is opposite of the side where scarfing initiates. In Fig. 8, the local static pressure P normalized by the entrance static pressure P_R is plotted against the axial position x normalized by the nozzle radius R. The wall pressure for the $M=3.0$ case remains at its initial value, indicating that Mach waves originating from the point where scarfing begins have not reached the opposite side of the nozzle. When the entrance Mach number is reduced to 1.8, cross flow develops in the internal flow since Mach waves originating from the point where scarfing initiates propagate into the internal flowfield. The cross flow acts to reduce the internal pressure as evidenced by the monotonic decrease in wall pressure. As a consequence of the reduced pressure acting on the nozzle's interior, the resultant thrust and moment components are reduced.

The boundary circumferential pressure distribution on a typical solution surface in the $M=1.8$ case is presented in Fig. 9. In this figure, the static pressure P normalized by the entrance static pressure P_R is plotted against the circumferential angle θ. The meridian at which scarfing initiates is denoted by $\theta=180$ deg, and the meridian corresponding to the results of Fig. 8 is denoted by $\theta=0$ deg. The initial portion of the pressure profile presented in Fig. 9 corresponds to the nozzle wall pressure in the internal flow. The pressure is highest at the $\theta=0$-deg meridian and monotonically decreases as θ increases. The solution surface intersects the exit lip at $\theta\cong 67$ deg. The remaining portion of the pressure profile corresponds to the free-pressure boundary; hence, the pressure for this portion of the profile equals the ambient pressure.

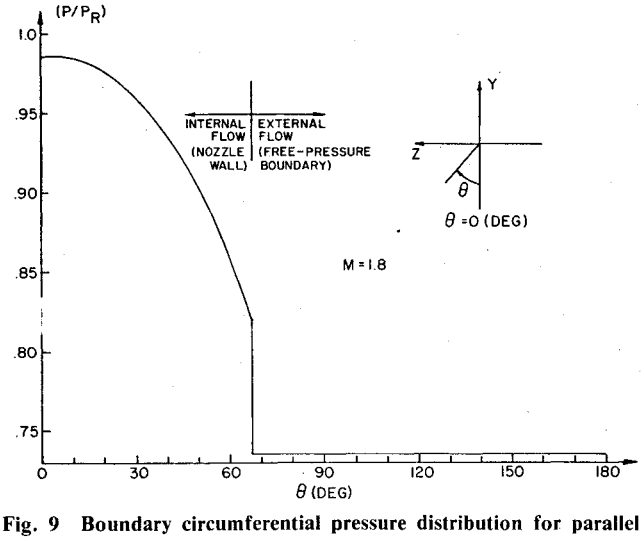

Fig. 9 Boundary circumferential pressure distribution for parallel wall nozzle.

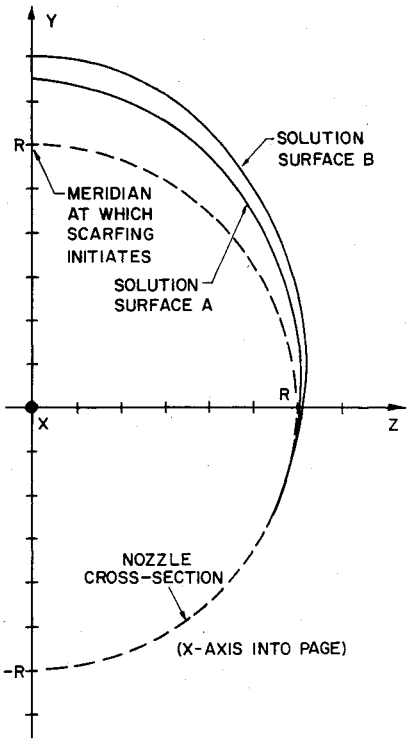

Fig. 10 Plume cross sections for parallel wall nozzle.

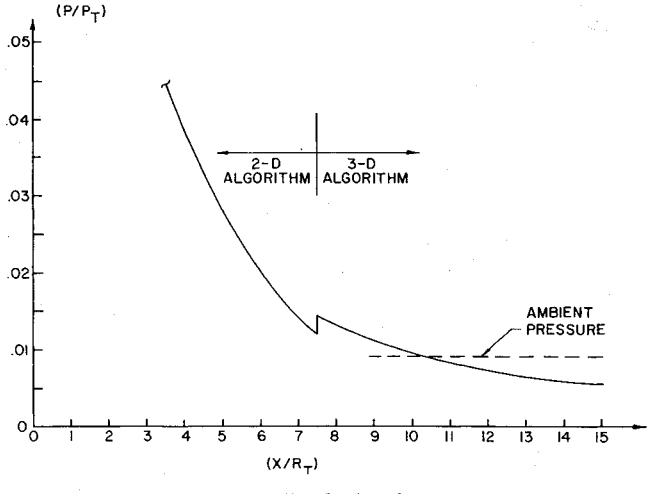

Fig. 11 Wall axial pressure distribution for 15-deg/13-deg conical nozzle configuration.

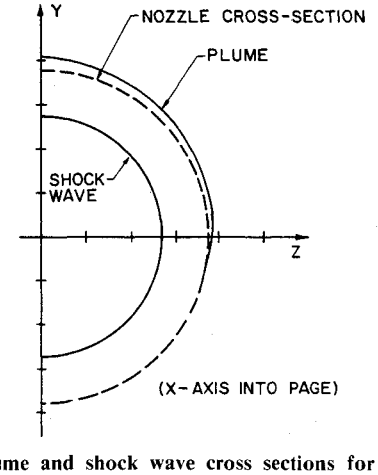

Fig. 12 Plume and shock wave cross sections for 15-deg/13-deg nozzle configuration.

Figure 10 illustrates the plume cross sections as viewed along the longitudinal axis of the nozzle for two different solution surfaces. Solution surface A is located at approximately ⅔ of the nozzle's length. Solution surface B is located very near the end of the nozzle. The plume expands asymmetrically with respect to the z axis and has it greatest radius lying in the meridian of the point at which scarfing was initiated.

The solution illustrated in Figs. 8-10 employed 9-radial and 15-circumferential stations in the computed sector which is the half-plane bounded by the y axis. The computation required 81 solution surfaces and approximately 25.5 min of CPU time on a CDC-6500/6600 computer system. This yields a computation rate of about 7.2 points/s on this system.

Computations were performed for a scarfed nozzle with a slope discontinuity. The nozzle configuration is composed of a circular arc throat attached to a 15-deg conical divergence. The contour downstream of the slope discontinuity is also a conical section with a 13-deg divergence angle. The required initial data were internally generated in the program. The slope discontinuity is located at $x=L$. The exit lip curve is generated by a plane cutting the nozzle. Scarfing initiates at $x=L$, the axial location of the slope discontinuity, and terminates at $x=2L$. The assumed thermodynamic model was that of a thermally and calorically perfect gas.

Figure 11 presents the wall axial pressure distribution on the meridian opposite of the side where scarfing initiates. In this figure, the local static pressure P normalized by the chamber stagnation pressure P_T is plotted against the axial position x normalized by the nozzle throat radius R_T. The initial portion of the profile is computed by the two-dimensional characteristics algorithm, whereas the final portion is determined by the three-dimensional flow algorithm. The wall pressure monotonically decreases until the slope discontinuity is encountered at which point a jump in the pressure profile occurs due to the presence of the oblique shock wave. After this point, the pressure monotonically decreases.

Figure 12 illustrates the plume and shock wave cross sections as viewed along the longitudinal axis of the nozzle at a solution surface which is located approximately at 80% of the nozzle's length. At this axial location, the plume has extended somewhat from the nozzle and the shock wave surface has been slightly distorted from a perfect circle. This computation required 20 solution surfaces and approximately 9.2 min of CPU time on a CDC-6500/6600 computer system. Nine radial and 15 circumferential stations were used in the computation.

Conclusions

A production-type computer program has been developed which is capable of analyzing the flowfield in a variety of axisymmetric scarfed propulsive nozzles. The computational technique is based on a bicharacteristic method devised for steady three-dimensional flow. For cases in which the nozzle contour has a slope discontinuity, the resulting shock wave system is computed using a three-dimensional discrete shock wave fitting procedure. The shock wave system is included in the computation until shock waves emanating from opposite sides of the nozzle approximately intersect.

Acknowledgment

This effort was sponsored by the U. S. Army Research Office under Contract DAAG29-78-G-0992.

References

[1] Vadyak, J. and Hoffman, J. D., "Calculation of the Three-Dimensional Supersonic Flow Field in Scarfed Propulsive Nozzles Using a Bicharacteristic Method with Discrete Shock Wave Fitting, Vol. I, Theoretical Development," School of Mechanical Engineering, Purdue Univ., W. Lafayette, Ind., Rept. TSPC-TR-80-01, 1980.

[2] Buchman, J. J. and Sternfeld, A. S., "Analysis of Problems Related to Thrust Reversal in Solid Propellant Motors," AIAA Paper 72-1110, 1972.

[3] Ransom, V. H., Hoffman, J. D., and Thompson, H. D., "A Second-Order Numerical Method of Characteristics for Three-Dimensional Supersonic Flow, Vol. I, Theoretical Development and Results," Air Force Aero Propulsion Laboratory, Wright-Patterson Air Force Base, Ohio, AFAPL-TR-69-98, 1969.

[4] Cline, M. C. and Hoffman, J. D., "The Analysis of Nonequilibrium, Chemically Reacting, Supersonic Flow in Three-Dimensions, Vol. I, Theoretical Development and Results," Air Force Aero Propulsion Laboratory, Wright-Patterson Air Force Base, Ohio, AFAPL-TR-71-73, 1971.

[5] Dash, S. M. and DelGuidice, P. D., "Analysis of Three-Dimensional Ducted and Exhaust Plume Flowfields," *AIAA Journal,* Vol. 16, Aug. 1978, pp. 823-830.

[6] Butler, D. S., "The Numerical Solution of Hyperbolic Systems of Partial Differential Equations in Three Independent Variables," *Proceedings of the Royal Society of London,* A255, 1960, pp. 232-252.

[7] Rusanov, V. V., "The Characteristics of General Equations of Gas Dynamics," *Zhurnal Vychistlitel 'noi matematiki: matematicheskoi fiziki,* Vol. 3, 1963, pp. 508-527.

[8] Vadyak, J. and Hoffman, J. D., "Calculation of the Flow Field in Supersonic Mixed-Compression Inlets at Angle of Attack Using the Three-Dimensional Method of Characteristics with Discrete Shock Wave Fitting," NASA CR-135425, 1978.

[9] Zucrow, M. J. and Hoffman, J. D., *Gas Dynamics,* Vols. I and II, Wiley, New York, 1977.